Appl. Phys. B (2013) 112:153–158
DOI 10.1007/s00340-013-5384-7

Applied Physics B
Lasers and Optics

Two-photon-excited photoluminescence and heating of gold nanorods through absorption of supercontinuum light

Wei Tao · Hongchun Bao · Min Gu

Received: 8 August 2012 / Accepted: 16 February 2013 / Published online: 6 March 2013

Abstract Most of lasers used for imaging and heating gold nanorods are single-wavelength lasers and their efficiency to interact with different gold nanorods is limited. In this study, we demonstrated that supercontinuum light could be a fast, effective and energy efficient excitation source for heating of gold nanorods. The photothermal effect and the heating speed of gold nanorods illuminated by a supercontinuum light and femtosecond pulses through two-photon excitation are experimentally studied through using transmission electron microscopy images and photoluminescence images of gold nanorods. It is found that the supercontinuum light improves the heating speed by 39 %, and melts 30 % more of gold nanorods compared with the femtosecond pulse excitation approach. The heating speed of gold nanorods by supercontinuum light depends not only on its polarization states, but also on the pulse width and numerical aperture of its focused beam. It has been found that the supercontinuum is more efficient in heating of gold nanorods, making it potentially valuable for clinical applications.

1 Introduction

Gold nanorods (NRs) have been widely used as multifunctional agents in plasmon-assisted imaging and photothermal treatments owing to their biocompatibility and unique optical properties [1]. The favorable property that their plasmon-resonant absorption can be shifted from the visible to near-infrared (NIR) range opens a window for deep tissue imaging. Gold NRs can also convert the light energy into heat via a series of photo-physical processes [2]. Recent studies have reported that gold NRs can be used for three-dimensional (3D) two-photon-excited photoluminescence imaging of cancer cells [3, 4], localized photothermal cancer therapy [5–7] and high-density optical data storage [8].

The heating speed and the heating efficiency of gold NRs directly affect the safety and the time required for the photothermal treatment, and the writing speed of optical data storage. Efficient and fast heating of gold NRs have been sought through optimizing the pulse width, the energy level, and the polarization state of an excitation laser beam [2, 9–11]. The impact of energy, pulse width, circular polarization and radial polarization of the excitation laser beam on the gold NR heating have been studied [2, 7, 9–11]. However, the broadband coherent supercontinuum (SC) source, which could be more efficient in heating gold NRs that usually show a finite size distribution, has not yet been investigated.

In this study, a linearly polarized coherent SC source is newly employed for heating gold NRs. The difference between the heating processes of gold NRs by the SC source and femtosecond pulses (FP) is studied. Our experiments show that the gold NRs can be heated faster by the broadband SC source and the SC source also shows the advantage in heating more gold NRs.

W. Tao · H. Bao · M. Gu (✉)
Faculty of Engineering and Industrial Sciences,
Centre for Micro-Photonics, Swinburne University
of Technology, Hawthorn, VIC 3122, Australia
e-mail: mgu@swin.edu.au

2 Experimental details

Figure 1a illustrates the central part of the experimental arrangement for a comparison of gold NR heating by a SC

source and a FP source. Gold NRs with an average aspect ratio of 4 and a maximal absorption at the wavelength of 780 nm were prepared using a seed-mediated growth method [12]. The gold NR solution was centrifuged several times and spin-coated onto a microscope cover glass as a NR sample. The NR sample, which was mounted on a 3D scanning stage, was scanned by a SC source or a FP source through an oil-immersion objective lens (100×, UplsApo, Olympus) with a numerical aperture (NA) 1.4. The scanning area of the sample was 100 μm × 100 μm and one scan of such the area took 120 s. The immersion oil nearly matched the index of the cover glass, providing a homogeneous optical medium between NRs and the objective. Photoluminescence (PL) signal (I_s) from the samples was separated from the reflected light (I_r) by a dichroic mirror and detected by a photomultiplier tube (PMT) after a filter. The illumination beam size and the effective NA of the focused beam can be adjusted by an iris.

Femtosecond pulses were generated directly from a Ti:Sapphire laser which produces 100 fs 80 MHz passive mode-locked ultra-short pulses. A SC source was obtained through propagating the FP in a 0.3-m long single-mode polarization-maintaining high-nonlinear photonic crystal fiber (HN-PCF, Crystal-Fiber) with a core diameter of 1.8 μm [13]. Figure 1b displays the structure of the HN-PCF and its polarization maintaining direction. The HN-PCF has two zero-dispersion wavelengths of 760 and 1,260 nm, and the HN-PCF is at the anomalous dispersion region between 760 and 1,260 nm. When the 800 nm pulses enter the HN-PCF, they undergo a transformation to form a high-order soliton and then convert into lower order solitons [13–15]. The output spectrum from the HN-PCF can be adjusted by changing the pulse width, the power, the wavelength and the polarization state of the pump FP [13]. The degree of polarization of the SC source, defined as $\gamma = (I_{max} - I_{min})/(I_{max} + I_{min})$, is displayed in Fig. 1c. The incident angle θ is the angle between the polarization direction of the incident FP and the polarization maintaining direction of the HN-PCF (Fig. 1b). The SC source is close to be linearly polarized when θ is 0° and 90°, corresponding to $\gamma = 0.83$ and 0.94, respectively (Fig. 1c). Figure 1d shows the extinction spectrum of gold NRs as recorded by a spectrophotometer. For gold NRs, the plasmon absorption splits into the longitudinal plasmon absorption and the transverse plasmon absorption corresponding to the oscillation of the free electrons along and perpendicular to the long axis of the gold NRs. The longitudinal plasmon absorption is much higher than the transverse plasmon absorption. An absorption spectrum of gold NRs clearly shows the presence of the two absorption maxima as shown in Fig. 1d. The longitudinal plasmon mode is excited by the electric field of light with the direction along the long axis of the gold NRs. Therefore, the light intensity along the longitudinal direction of NRs is effective in exciting the longitudinal plasmon mode and generating heat in gold NRs.

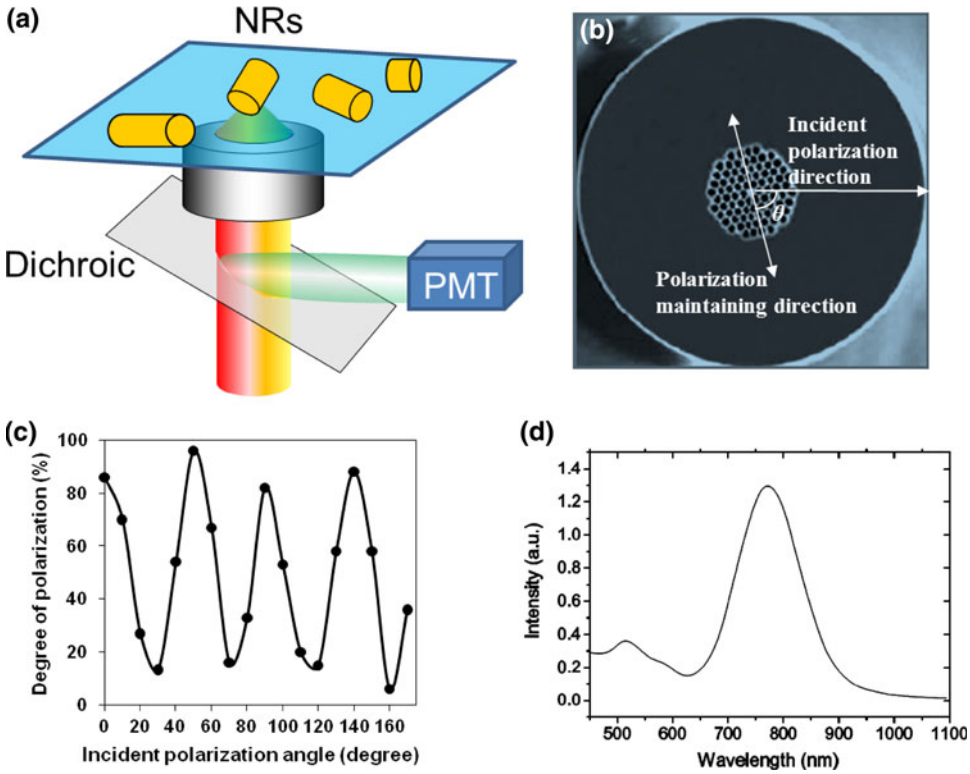

Fig. 1 **a** Schematic diagram of the experimental set-up for excitation of the SC source or the FP on NRs. *DM* dichroic mirror. **b** Structure of the HN-PCF. *Arrows* indicate fiber polarization maintaining direction. **c** Degree of polarization of the SC source (γ) versus the polarization direction of the incident FP (θ). **d** The absorption of gold NRs with a longitudinal plasmon mode centered at 780 nm and a transverse mode centered at 515 nm

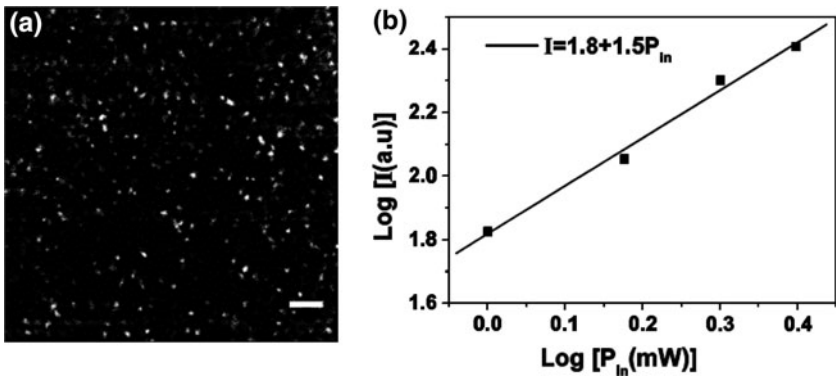

Fig. 2 **a** The two-photon-excited PL imaging of gold NRs by SC. *Scale bar* 10 μm. **b** Quadratic dependence of two-photon-excited PL intensity on excitation power

3 Results and discussion

The PL image of gold NRs under the irradiation of the SC is shown Fig. 2a. Gold NRs give strong PL excited by the SC. The dependence of PL intensity against the incident power on a logarithm scale is revealed in Fig. 2b. Like optical pulses with the single central wavelength [7, 16], the logarithm scale plot of the PL intensity against the incident power fits a straight line with a gradient of 1.5, which is close to 2, indicating the generated PL from gold NRs excited by the SC is mainly a two-photon excitation process.

The PL images of the NRs excited by a linearly polarized SC source beam ($\theta = 0°$) after the NRs being scanned for 1, 5, 15 and 20 times are revealed in Fig. 3a, b, c and d, respectively. The PL intensity of most gold NRs drops with the increase of the scan number, while that of some gold NRs (arrowed) does not show an obvious change. The absorption of the SC source transforms the shape of NRs into shorter rods or spherical particles [2]. Therefore, the absorption peak and the absorption intensity of the longitudinal plasmon band of the transformed NRs can be blue shifted and decreased. As a result, the PL intensity from the NRs declines. Some NRs show no obvious change of the PL intensity because their elongating direction is perpendicular to the polarization direction of the SC source and they absorb little of the SC source. The average PL intensity of NRs decreases with the increase of the scan number, as shown in Fig. 3e. The declining speed of the average PL intensity, which is defined as the ratio of the drop of the average PL intensity over the scan number, directly reflects the heating speed of NRs. Figure 3e shows that the average PL intensity declining speed of the NRs is 10.5.

To compare the heating speed of gold NRs between the SC source and the FP, we measured the average PL intensity declining speed of gold NRs excited by the SC source and the FP. The excitation power on the samples for both cases is 2 mW. Figure 4a shows the average PL intensity declining speed of NRs induced by the SC source

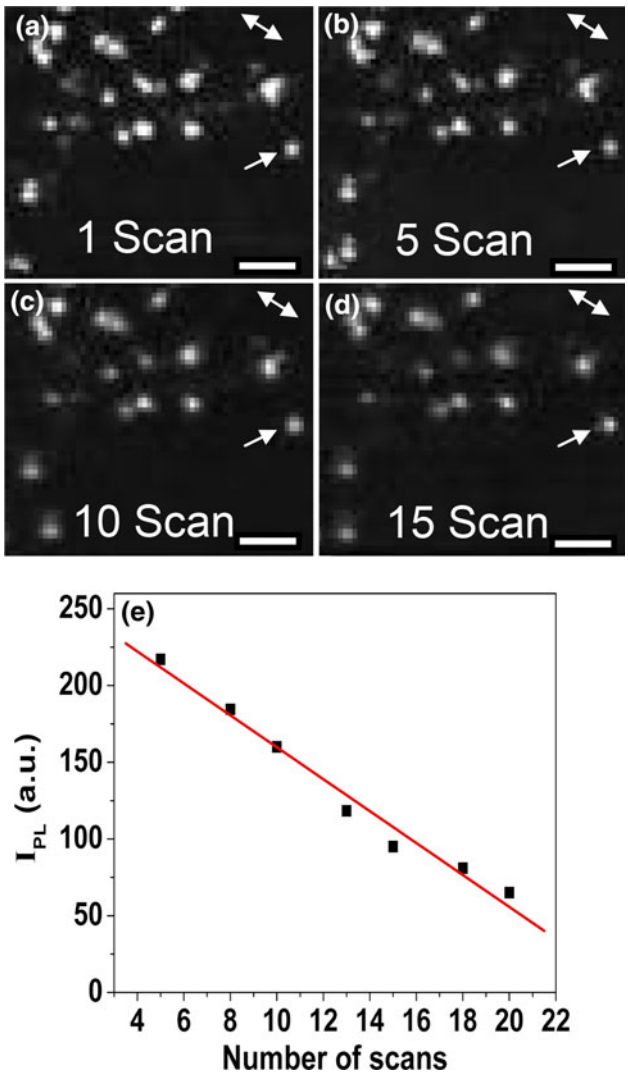

Fig. 3 The PL images of gold NRs after **a** 1 scan, **b** 5 scans, **c** 15 scans and **d** 20 scans by the linearly polarized SC source. *Bidirectional arrows* indicate polarization direction of the SC source. *Scale bar* 5 μm. **e** Average PL intensity of gold NRs, I_{PL}, as a function of the scan number

and by the FP as the effective NA of the focused beam is 0.75, 0.95 and 1.4, respectively. The different NAs are

obtained by changing the aperture of the iris. The PL intensity declining speed of the NRs induced by the SC source is 26, 39 and 35 % faster than that by the FP for the NA 0.75, 0.95 and 1.4, respectively.

The influence of the incident polarization states of the SC source on heating of the gold NRs is illustrated in Fig. 4b, which shows the PL intensity declining speed of NRs scanned by the SC source when θ is 0°, 45° and 90°, respectively. The heating speed for $\theta = 0°$ and $\theta = 90°$, where the generated SC source from the HN-PCF is close to be linearly polarized (Fig. 1c), is faster than that for $\theta = 45°$. In the heating process, only the light intensity along the longitudinal direction of gold NRs is effective in melting. For the linearly polarized SC source, all the light intensity can be aligned with the longitudinal direction of NRs. Since gold NRs are randomly orientated, there are always a certain number of gold NRs with their orientation direction along the linear polarization direction of the incident light in 0° and 90° cases. Those gold NRs have the maximum absorption of photons. On the other hand, as θ is 45°, the light intensity is dispersed on all directions ($\gamma = 0.12$, Fig. 1c). For every particular direction, the light intensity is weak. Although more gold NRs could absorb some photons, the absorption of a given gold NR is less than the maximum absorption in 0° and 90° cases. Compared with the spectrum as $\theta = 0°$ (Fig. 4c), more components move to wavelengths >850 nm for $\theta = 90°$ (Fig. 4e), which is outside the absorption region of most NRs. Therefore, the heating speed at $\theta = 90°$ is lower than that at $\theta = 0°$. The heating speed with the effective NA 1.4 is approximately 19 and 54 % faster compared with that for NA of 0.95 and 0.75, respectively. The light intensity in the small focus spot of the high NA beam is higher and the amount of the energy absorbed by the gold NRs is proportional to the focused light intensity [17]. However, as NA is over 0.6, the polarization of the focused light beam starts to depolarize [18]. Depolarization would slightly reduce the absorption increase; however, the decrease of the photon absorption due to the depolarization is much less than the increase of photon absorption due to the intensity increase of the focused light beam as NA increases [18]. Therefore, the intensity increase of the focused light beam dominates the increase of the photon absorption as NA increases. Although the use of other polarization states [11] or their combinations [19] of the laser beam may enhance the interaction of the light with NRs in an arbitrary orientation, the broadband feature of a SC source can enhance the depolarization in the focus of a high NA objective.

Figure 5a–c shows the transmission electron microscopy (TEM) images of the NRs prior to the laser irradiation, after scanning by the SC source and the FP for 10 times at a

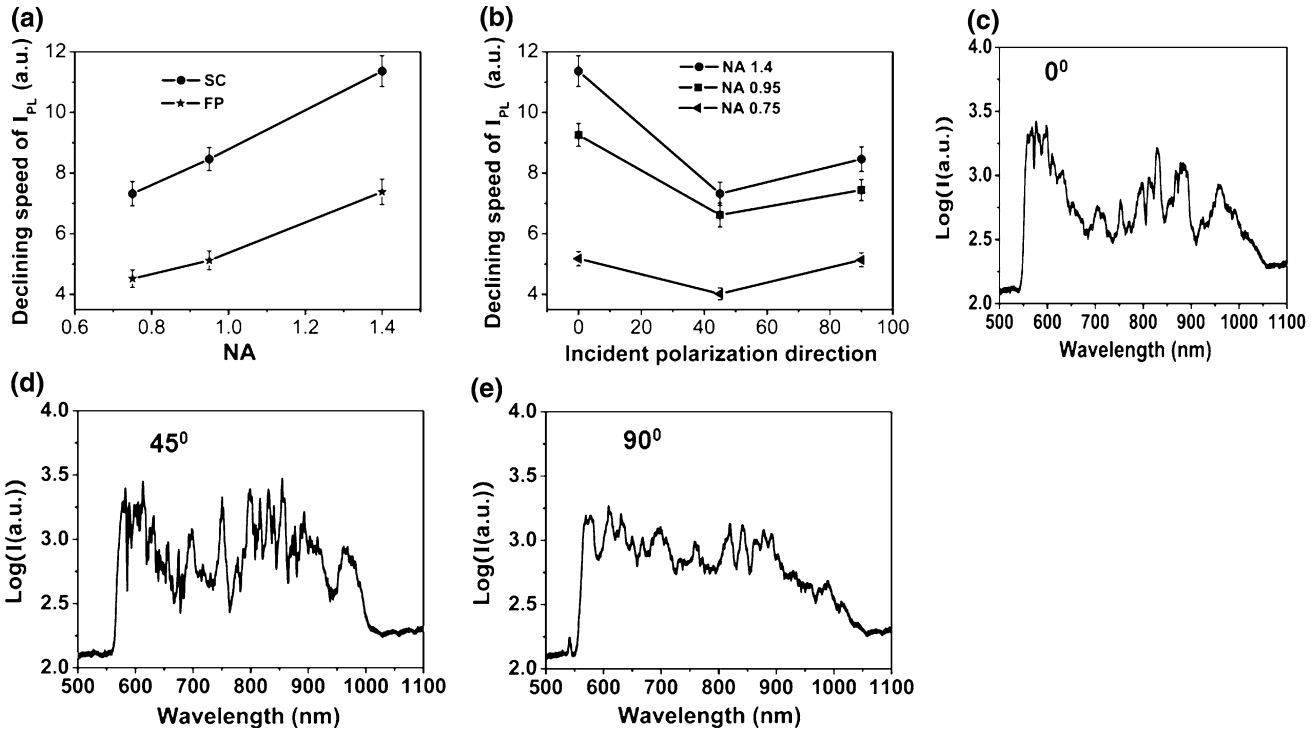

Fig. 4 **a** Dependence of the PL intensity declining speed of gold NRs on the effective NAs of FP and SC beams. **b** PL intensity declining speed of gold NRs using the SC source versus the polarization directions of the incident FP to the polarization maintaining direction of the HN-PCF. The *error bars* in **a** and **b** denote one standard deviation from 5 replicates. **c–e** The spectrum of the SC source when $\theta = 0°, 45°, 90°$

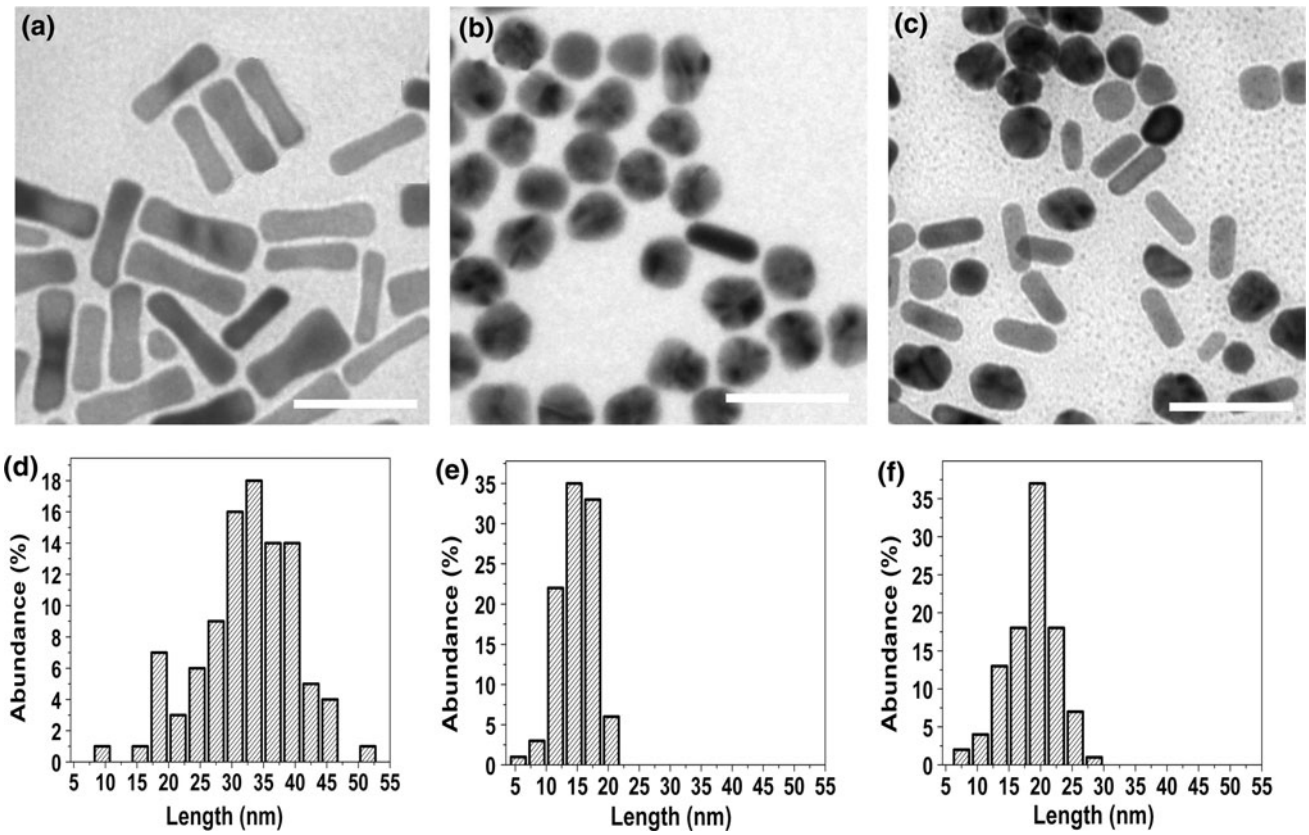

Fig. 5 **a** TEM images of original gold NRs. **b**, **c** TEM images of the NRs after irradiation with the SC source and the FP for 10 scans. The size distribution of the NRs before (**d**) and after irradiation with the SC (**e**) source and the FP (**f**). The *scale bars* of all the TEM images are 50 nm

given power of 2 mW. During scanning by the SC source or the FP, the absorption of photon energy induced the process of electron–photon coupling and caused the shape transformation of gold NRs [2, 8, 17]. This process results in a variation of the aspect ratio distribution of NRs. A comparison of Fig. 5b with Fig 5c shows that more NRs melted and the melted NRs were shorter in the case that NRs were excited by the SC source. This is confirmed quantitatively by a statistical size distribution of a large number of NRs before and after exposure to the light sources (Fig. 5d–f). The mean lengths of the NRs after illuminated by the SC source (Fig. 5e) and the FP (Fig. 5f) are 15 and 19 nm, respectively. In addition, 80 % of the NRs were found to be transformed their shape into shorter and wider rods or spherical particles after the excitation by the SC source, while only 50 % were in the FP excitation case. The NRs have a broad distribution of aspect ratios (or lengths, Fig. 5d) and the different aspect ratios of the NRs have different absorption wavelengths. The narrow spectral bandwidth of the FP (15 nm in the experiment) can only heat a small population of NRs which have the peak absorption wavelength matching with the wavelength of the FP. On the other hand, the SC source can heat a large number of the NRs because the broadband SC source can cover the different absorption wavelengths of the NRs with the different aspect ratios.

4 Conclusion

In summary, we report that photothermal heating of gold NRs induced by the SC source is faster and more effective than that of a FP excitation and the heating speed is strongly dependent on the polarization directions of the illumination light and the NA of the focused beam. High NA focusing by the linearly polarized SC beam is found to be more efficient and fast on heating of gold NRs. The SC source could be advantageous in melting gold NRs as they are utilized in plasmon-assisted photothermal therapy and high-density optical data storage.

Acknowledgments This work was partly supported by the Australian Research Council (ARC) Laureate Fellowship scheme (FL100100099). The authors would like to thank Dr. Jing Liang Li for his assistance in the preparation of the gold NR samples.

References

1. L. Tong, Q. Wei, A. Wei, J.X. Cheng, Photochem. Photobiol. **85**, 21 (2009)
2. S. Link, C. Burda, M.B. Mohamed, B. Nikoobakht, M.A. EI-Sayed, J. Phys. Chem. A **103**, 1166 (1999)
3. H. Wang, T.B. Huff, D.A. Zweifel, W. He, P.S. Low, A. Wei, J. Cheng, PNAS **102**, 15752 (2005)
4. N.J. Durr, T. Larson, D.K. Smith, B.A. Korgel, K. Sokolov, A. Ben-Yakar, Nano Lett. **7**, 941 (2007)
5. R.R. Letfullin, C. Joenathan, T.F. George, V.P. Zharov, Nanomedicine **1**, 473 (2006)
6. C.L. Didychuk, P. Ephrat, A.C. Reig, S.L. Jacques, J.J.L. Carson, Nanotechnology **20**, 195102 (2009)
7. J.L. Li, D. Day, M. Gu, Adv. Mater. **20**, 3866 (2008)
8. P. Zijlstra, J.W.M. Chon, M. Gu, Nature **459**, 410 (2009)
9. S. Link, M.A. EI-Sayed, J. Chem. Phys. **114**, 2362 (2001)
10. S. Inasawa, M. Sugiyama, Y. Yamaguchi, J. Phys. Chem. B **109**, 9404 (2005)
11. H. Kang, B. Jia, J. Li, D. Morrish, M. Gu, Appl. Phys. Lett. **96**, 063702 (2010)
12. T.K. Sau, C.J. Murphy, J. Am. Chem. Soc. **126**, 8648 (2004)
13. B.J. Chick, J.W.M. Chon, M. Gu, Opt. Express **16**, 20099 (2008)
14. M. Lehtonen, G. Genty, H. Ludvigsen, Appl. Phys. Lett. **82**, 2197 (2003)
15. J.C. Knight, J. Broeng, T.A. Birks, PStJ Russell, Science **282**, 1476 (1998)
16. M. Gu, H. Bao, J.L. Li, J. Biomed. Opt. **15**, 050502-1-3 (2010)
17. P. Zijlstra, J.W.M. Chon, M. Gu, Phys. Chem. Chem. Phys. **11**, 5915 (2009)
18. H. Kang, M. Gu, J. Appl. Phys. **112**(8), 083106 (2012)
19. X. Li, T. Lan, C. Tien, M. Gu, Nat. Commun. **3**, 998 (2012)